


# Drop-weight testing of slender reinforced concrete beams

Noosha Madjlessi<sup>1</sup> | Demitrios M. Cotsovos<sup>1</sup>  | Mojtaba Moatamedi<sup>2</sup>

<sup>1</sup>Institute of Infrastructure and Environment, Heriot-Watt University, Edinburgh, UK

<sup>2</sup>Faculty of Technology, Art and Design, Oslo Metropolitan University, Oslo, Norway

## Correspondence

Demitrios M. Cotsovos, Institute of Infrastructure and Environment, Heriot-Watt University, Edinburgh, EH14 4AS, UK.

Email: d.cotsovos@hw.ac.uk

## Abstract

The work presented herein sets out to investigate experimentally, via drop-weight testing, the behavior of slender reinforced concrete (RC) beam specimens under impact loading. During testing, the behavior of each specimen is established through the combined use of conventional instrumentation and a high-speed video camera. The primary objective of this work is to investigate the reasons that trigger the observed shift in specimen behavior (compared to that established from static tests) with increasing levels of applied loading rate and intensity. Analysis of the test data reveals that during drop-weight testing only a portion of the element span reacts to the applied load (as indicated by the deformation and cracking profiles recorded) which in turn affects the mechanics underlying specimen behavior and therefore, significantly influencing the mode of failure ultimately exhibited. The observed localized response becomes more prominent by increasing the loading rate and intensity of the imposed impact loading. In addition to the above, the strain-rate sensitivity of the material properties of concrete does not appear to have a significant effect on the behavior of the specimens tested. The aforementioned observations appear to be in conflict with current design practice raising questions concerning the effectiveness of the design solutions produced.

## KEYWORDS

cracking, drop-weight testing, dynamic response, impact, loading rate, reinforced concrete, slender beams, strain rate, wave propagation

## 1 | INTRODUCTION

In recent years, there has been an increasing realization that there is a need for reinforced concrete (RC) structures to achieve an intended level of resilience in order to

sustain the action of loads induced at rates and intensities significantly higher than those already considered by the available design standards. Such loads, which are characterized by short duration (of few milliseconds) and high intensities (significantly higher than the load-carrying capacity of the structural components established from static and seismic [shake table] tests), can be generated during the collision of vehicles or other objects with structural components (beams, columns, walls, or slabs). It has been established, both experimentally<sup>1–12</sup> and numerically<sup>3,5,8,9,13–20</sup> that, once certain thresholds of the rate and intensity of the applied loading are surpassed,

All data referred to in this publication are available upon request from the corresponding author

Discussion on this paper must be submitted within two months of the print publication. The discussion will then be published in print, along with the authors' closure, if any, approximately nine months after the print publication.

This is an open access article under the terms of the Creative Commons Attribution License, which permits use, distribution and reproduction in any medium, provided the original work is properly cited.

© 2021 The Authors. *Structural Concrete* published by John Wiley & Sons Ltd on behalf of International Federation for Structural Concrete.

the dynamic response of RC beams under impact loading exhibits significant departures from that established from static tests. The available numerical and test data reveal that, with increasing loading rates, RC beams exhibit a more localized response, since the portion of the beam reacting to the external load reduces in length as cracking (and often failure) occurs prior to the generated stress waves reaching the supports. This phenomenon, which is evident from the specimen crack pattern, combined with the inertia forces developing along the specimen span underlies the mechanisms governing RC structural response under impact loading.<sup>15,21</sup>

A review of the available test data reveals that the above phenomenon is more pronounced in the case of slender RC beams with a shear-span to depth ratio ( $\alpha_v/d$ ) greater than five. Under static loading, such elements (even when containing the nominal amount of shear links) exhibit ductile behavior, with flexural cracking gradually spreading along the whole element span, with those in the mid-span region penetrating deep into the compressive zone and ultimately resulting in a flexural mode of failure.<sup>22</sup> When subjected to impact loading, slender RC beams tend to exhibit more localized response and cracking which often leads to brittle, if not explosive modes of failure, while, at the same time, the sustained load is higher than its static counterpart<sup>15,18</sup>.

The causes underlying the above differences in structural behavior do not appear to be as yet fully understood. Since the early 1980s, it has been widely considered that the response of RC beams to impact loading is linked with “strain-rate sensitivity” of concrete at the material level; in fact, strain-rate sensitivity underlies current code specifications for the design of military structures.<sup>23</sup> The validity of this concept has been challenged in recent years by demonstrating numerically that it is possible to obtain realistic predictions of RC structural response under impact loading without considering strain-rate sensitivity at the material level.<sup>15,18,21</sup> However, experimental evidence in support of these numerical findings is currently lacking. The available test data is often restricted to measurements of the contact force, the corresponding mid-span deflections and the support reactions, as well as observations of the crack-patterns along the span of the specimen. Such data are insufficient for studying in detail the mechanics underlying RC structural behavior under impact loading as information on the changes of deformation profile and crack formation throughout the loading process is often scarce.

To this end, the work described herein is intended to produce experimental information on features of structural behavior that will help to improve our understanding of the mechanics underlying the behavior exhibited by slender RC beams when subjected to drop-weight loading. Such information will include measurements of the generated impact

and reaction forces, of displacements along the element span and of the strain ( $\epsilon$ ) and strain rate ( $\dot{\epsilon}$ ) at specific locations throughout the loading process. The cracking and deformation profiles of the specimens at different stages of the loading process, as well as the modes of failure, will also be established as these are linked with the internal state of stress underlying the observed and measured structural behavior. The above will be achieved through the use of conventional instrumentation (e.g., LVDTs, accelerometers, strain-gauges, and load-cells) combined with a high-speed (HS) video camera, which has been proven to provide accurate measurements capable of describing in detail specimen behavior throughout the loading process.<sup>10</sup>

## 2 | TEST PROGRAMME

The work presented involves the testing (summarized in Table 1) of six simply supported beams. From the table, it can be seen that all beams, apart from one tested under static loading, were subjected to impact loading. Two types of beams were used (type A and type B) with the letter (A or B) indicating the beam type being followed by a number merely indicating the sequence of testing. It is noted that type B beams included less top longitudinal reinforcement and stirrups compared to their type A counterparts (see Figure 1) in an attempt to assess the effect of these parameters on *the* behavior exhibited during drop weight testing. Table 1 also includes information related with the impact tests. Such information includes the height ( $H_i$ ) from which the mass was dropped, the velocity ( $v_i$ ) of the drop mass at the time of contact with the specimen and the type of pad placed on the impacted region which is discussed later. From the table, it can also be seen that the specimens subjected to impact loading were tested more than once, the reasons for this being discussed later.

### 2.1 | Specimen design details

The geometry and reinforcement details of the specimens are shown in Figure 1. From the figure, it can be seen that all specimens have the same geometry and only differ as regards the reinforcement details. They have a rectangular cross section 200 mm high  $\times$  100 mm wide; their full length is 3000 mm and their clear span 2700 mm. The longitudinal reinforcement of type A beams comprises two 10 mm diameter top bars and two 12 mm diameter bottom bars, whereas their transverse reinforcement consists of 10 mm diameter stirrups at a spacing of 200 mm. Type B beams differ from their type A counterparts in that their top longitudinal reinforcement and



Beam type	Test type	Test no.	$H_i$ (m)	$v_i$ (m/s)	Pad (mm)		
A	A1	Static	1	N/A	Steel (40 mm)		
		Impact	2	0.5	3.16	Ply (15 mm)	
	A2		3	1	4.42		
			4	1	4.42		
		A3		5	1	4.42	Steel (40 mm)
				6	1.5	5.42	
B	B1		7	1	4.42		
			8	1.5	5.42		
			9	1	4.42		
	B2		10	1.5	5.42	Ply (35 mm)	
			11	2	6.26		
	B3		12	2	6.26		
			13	2	6.26		

TABLE 1 Summary of the experimental programme

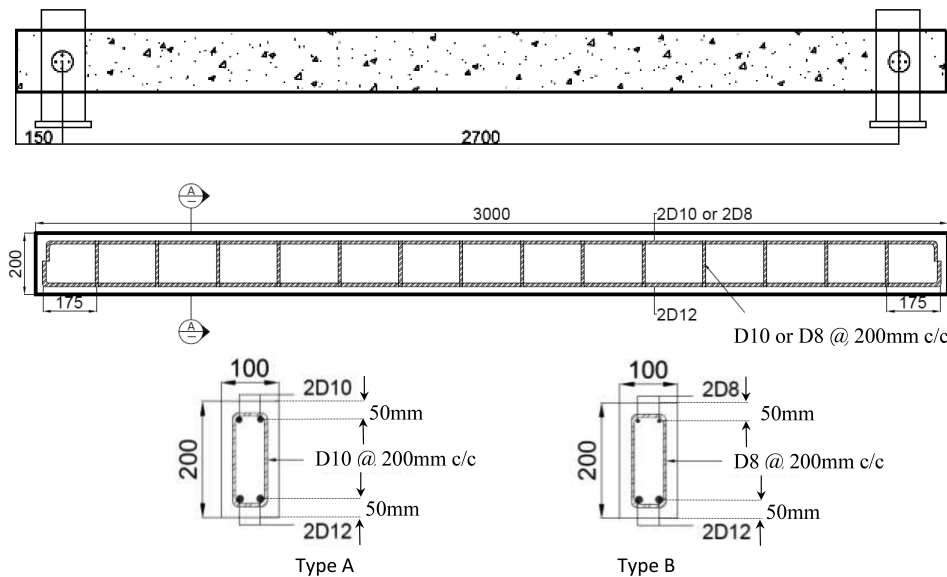


FIGURE 1 RC beam specimen investigated (all dimensions in mm)

TABLE 2 Steel reinforcement mechanical properties

Rebar diameter size (mm)	12	10	8
$f_y$ (MPa)	566	609	503
$f_u$ (MPa)	684	727	640
$E_s$ (GPa)	200	200	200
$\epsilon_y$	0.00283	0.003045	0.002515
$\epsilon_u$	0.12	0.14	0.11

stirrups have an 8 mm (rather than 10 mm) diameter. In all cases, the distance of the geometric centre of the longitudinal reinforcement bars from the top and bottom end faces closest to them was 50 mm.

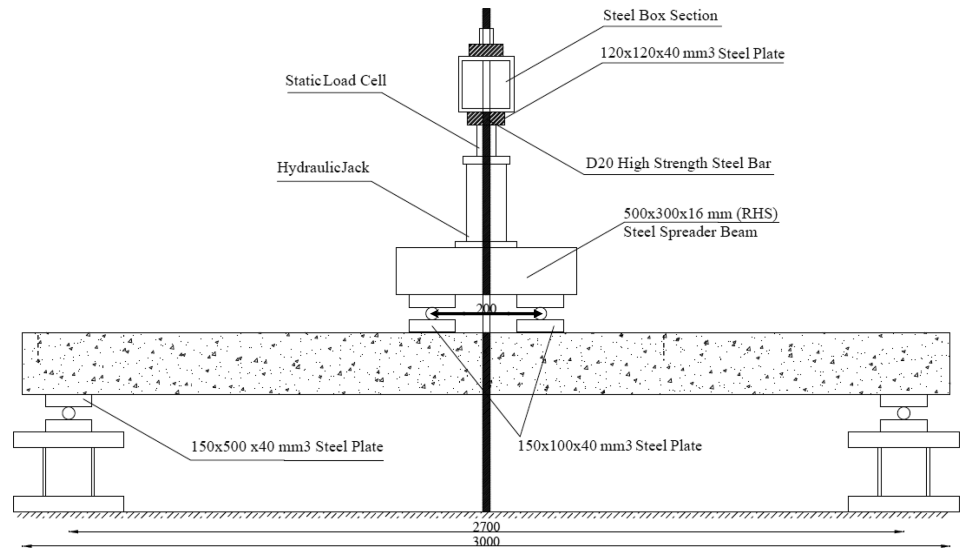
As regards concrete, its 28 day compressive strength established from tests on cubes with 100 mm

side was 27 MPa, whereas its splitting strength established from tests on cylinders with length of 300 mm and diameter of 100 mm was 1.88 MPa. The mechanical properties of the steel bars used are provided in Table 2. In accordance with Eurocode 2<sup>24</sup> the flexural capacity of the specimens (Type A and

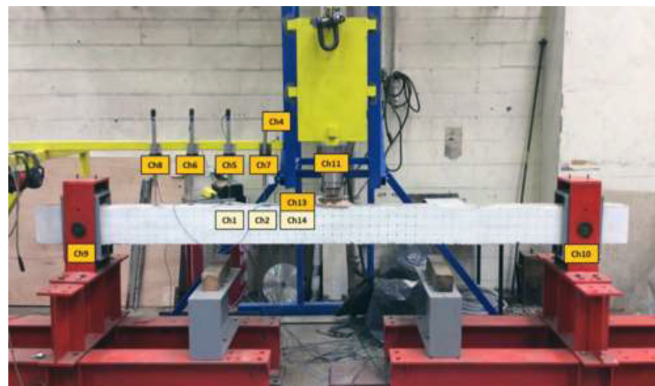
Type B) is approximately  $M_f = 16 \text{ kN}\cdot\text{m}$  and the corresponding shear is  $V_f = M_f/a_v = 12.8 \text{ kN}$ . The shear capacity of the Type A and Type B specimens

under static loading conditions is predicted to be 161 and 85 kN respectively (the latter values being significantly higher than  $V_f$ ).

**FIGURE 2** Experimental setup used for establishing the behavior of specimen A1 under static loading (the side of the steel plates with a length of 150 mm was always placed along the span of the beam). All dimensions are in mm



(a)



- Ch1 Accelerometer
- Ch2 Accelerometer
- Ch3 -
- Ch4 Accelerometer
- Ch5 LVDT
- Ch6 LVDT
- Ch7 LVDT
- Ch8 LVDT
- Ch9 Load Cell
- Ch10 Load Cell
- Ch11 Load Cell
- Ch12 -
- Ch13 Strain gauge
- Ch14 Strain gauge

(b)

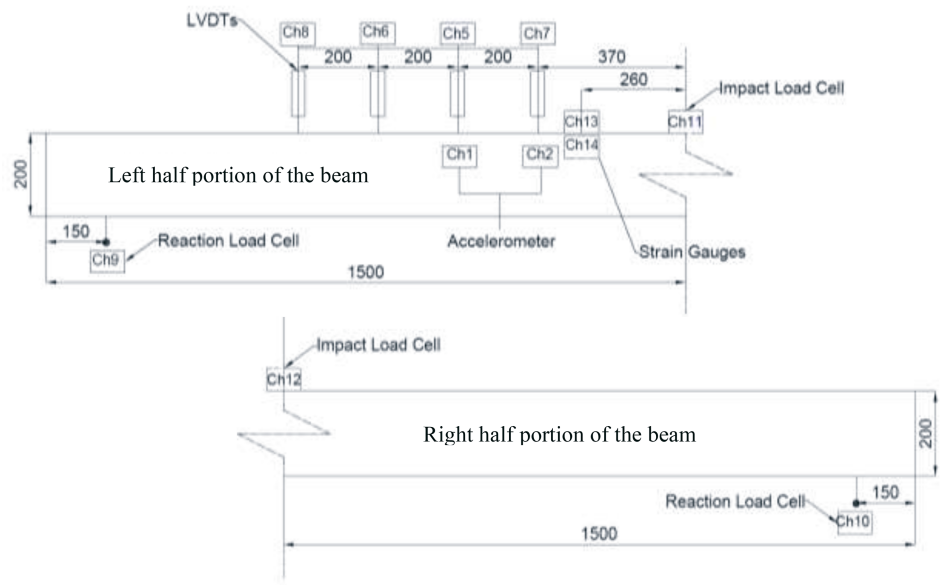


**FIGURE 3** (a) Experimental setup used for conducting drop-weight testing and (b) location of instruments used to record the behavior of the RC beam specimens

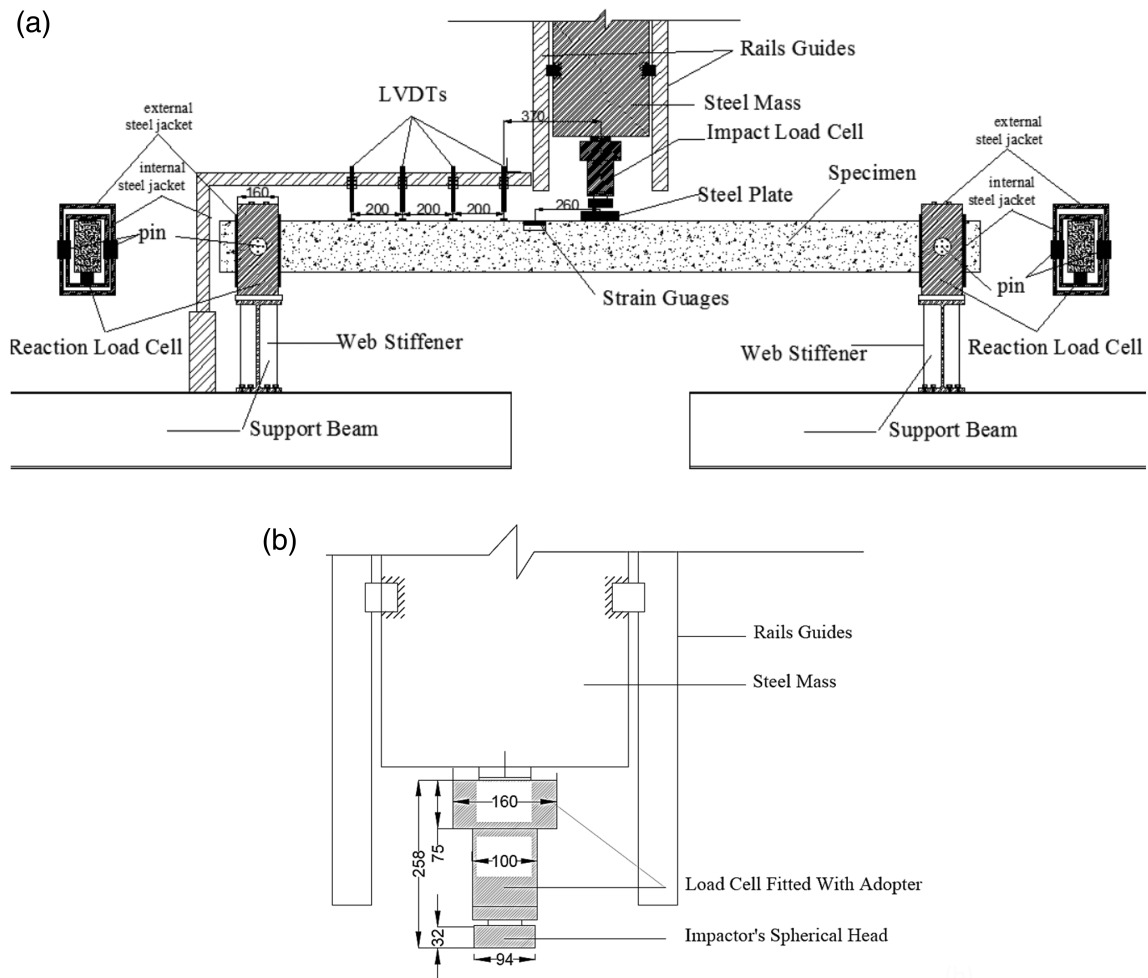


FIGURE 4 (a) Layout of the experimental setup used for conducting drop-weight testing on the RC beam specimens and (b) detailed drawing of the geometry of the impactor used

## 2.2 | Setup for static testing

As indicated in Table 1, specimen A1 was subjected to static loading. Figure 2 provides a schematic representation of the test set up used for this purpose. Through the use of a 300 kN hydraulic jack, the load was applied in the form of displacement increments monotonically increasing to failure. As indicated in Figure 2, the jack was placed between a steel beam positioned above it and the strong floor through two high-strength steel bars with a diameter of 20 mm. Via a short rigid spreader beam, the applied load was transferred to the specimen at two locations situated at a small distance (of 207.5 mm) from either side of the specimen mid span. Steel plates were placed as indicated in the figure at the loading points and the supports in order to effectively distribute the concentrated loads and reactions so as to avoid the development of high-stress concentrations in these regions that could cause localized cracking and premature failure of the

specimen. During testing, the deflections at the bottom face of the specimen at mid span were measured through the use of a dial gauge. In addition, the crack patterns at different levels of loading were marked and photographed.

## 2.3 | Setup for drop-weight testing

The drop-weight testing rig is presented in Figures 3 and 4; it was capable of delivering a steel drop mass (impactor) of 124 kg onto the mid-span region of the specimens from a maximum height of 4 m. All specimens were subjected to multiple drop-tests in order to study the behavior exhibited during consecutive impacts. At their ends, the specimens were placed into steel jackets which were allowed to rotate as shown in Figures 3 and 4. Steel pads were placed at the supports of the beams to avoid the development of high-stress concentrations that could lead

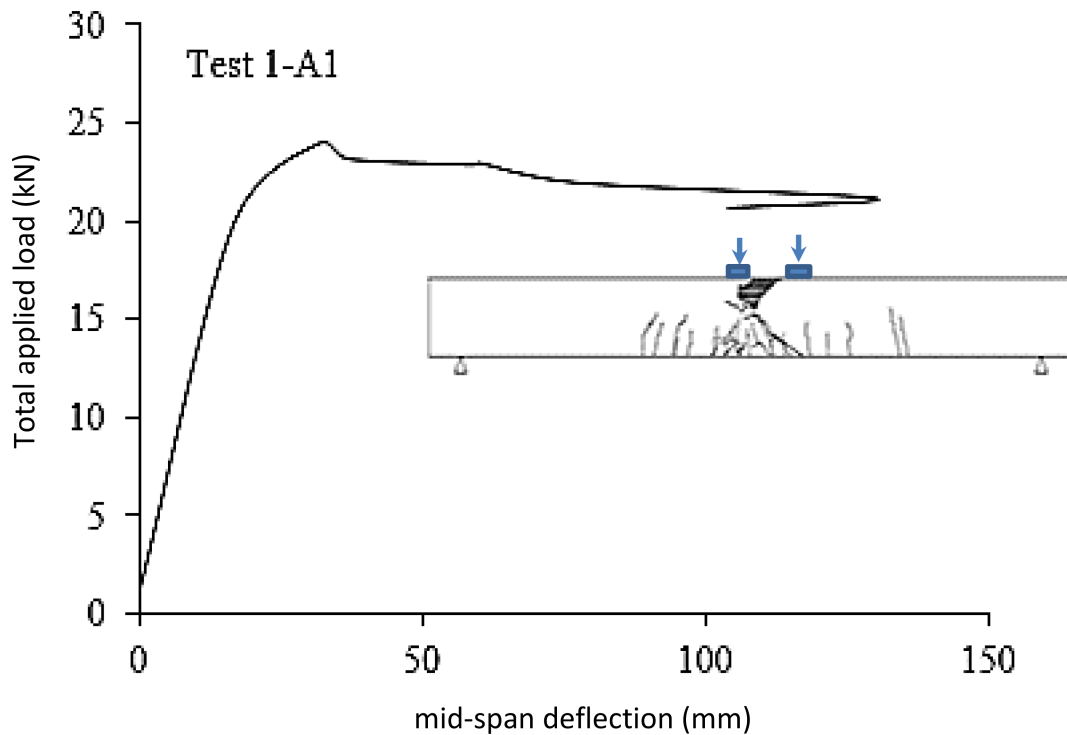


**FIGURE 5** Curve describing the variation of the total applied load with midspan displacement accompanied by a schematic representation of the crack patterns established experimentally for the case of specimen A1 (type a) when subjected to static 4-point bending testing

to localized cracking and possibly premature failure in these regions. Plywood or steel pads were also used in the impacted regions (between the impactor and the beam) to moderate the level of damage sustained at the top surface of the specimen during each collision and, to some extent, control the loading rate and intensity of the impact load generated during each drop test. The steel pads were used in order to achieve impact loads characterized by higher values of loading rate ( $\dot{P}$ ) and intensity ( $\max P_d$ ) (high-intensity impact), whereas plywood pads were used to reduce the loading rate and intensity of the contact force generated in the impact region (moderate-intensity impact). Figure 3 shows the position of the instruments used along the span of the specimens. These instruments consist of:

- four linear variable differential transducers (LVDTs) with a stroke of  $\pm 75$  mm mounted at different locations along the element span to measure the vertical displacement exhibited at these points. The LVDTs used had a maximum measuring frequency of 35 kHz. They were labeled Ch-5, Ch-6, Ch-7, and Ch-8 and mounted on a steel frame supported independently to the rest of the setup.
- Two dynamic load cells, labeled Ch-9 and Ch-10, were placed underneath each support to measure the

variation of the reaction forces generated with time. An additional 2000 kN dynamic load-cell (labeled Ch-11) was attached to the bottom of the drop-weight and used to measure the impact (contact) force generated during the collision of the drop-mass with the specimen.

- All specimens in tests 5 to 13 were fitted with two strain gauges. One of the strain gauges was mounted on the top surface of the beam (being in compression) at a distance of 260 mm from the mid-span (labeled Ch13). The second strain gauge was attached 50 mm below the first one on the side of the specimen (labeled Ch14).
- The data acquisition system used was capable of recording data at a sampling rate of 35 kHz per channel.

Finally, a high-speed camera set to record at a rate of 2000 frames per second (*fps*) was also used. The camera was used for purposes of comparison with the measurements obtained from the instrumentation described earlier and for compensating for the occasional loss of measurements due to damage of the instrumentation. The photographic evidence was found to provide, throughout the loading process, a more detailed description of the specimen behavior in the impact region by

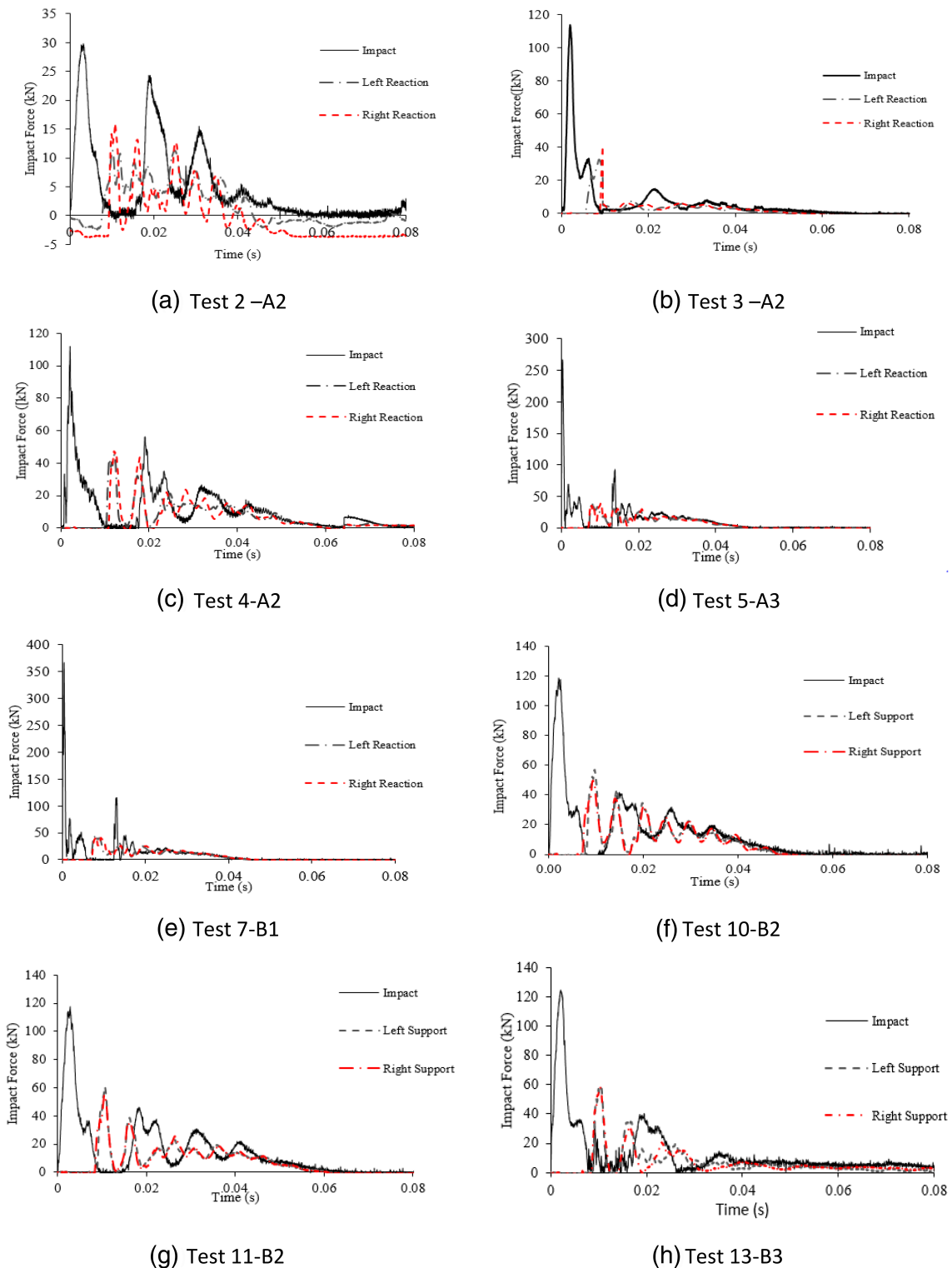


FIGURE 6 Impact and reaction force time histories recorded during different drop-weight tests at different loading rates and intensities

tracking the movement of the points marked in the form of a grid on the side surfaces of the specimen, of the pad and of the impactor. This was achieved by digitizing the video recordings through the use of appropriate tracking software.<sup>25</sup>

### 3 | SPECIMEN BEHAVIOR UNDER STATIC LOADING

The behavior of beam specimen A1 under static loading is presented in Figure 5 in the form of a curve describing



TABLE 3 Key characteristics established from the curves (see Figure 8) describing time-histories of the impact and reaction forces generated during drop weight testing.

Test no.	Pad	H (m)	maxP <sub>d</sub> (kN)	t <sub>P</sub> (ms)	Ṗ (kN/ms)	maxR <sub>d,10</sub> (kN)		maxR <sub>d,10</sub> /maxP <sub>d</sub>		t <sub>r,10</sub> (ms)		Δt <sub>10</sub> = t <sub>r</sub> - t <sub>m</sub> (ms)	
						Left support	Right support	Left support	Right support	Left support	Right support	Left support	Right support
<b>A1</b> 40 mm steel (Static)													
A2	15 mm ply	0.5	29.6	2.8	10.57	11.3	15.9	0.38	0.54	10.54	9.67	7.74	6.87
3	15 mm ply	1	113.7	1.5	75.8	32.5	40.5	0.29	0.36	9.21	9.24	7.71	7.74
4	15 mm ply	1	112.3	1.3	86.38	45.4	47.3	0.40	0.42	12.81	12.23	11.51	10.93
A3	40 mm steel	1	267.0	0.36	741.67	40.31	37.0	0.15	0.14	7.76	7.93	7.4	7.57
6	40 mm steel	1.5	—	—	—	—	—	—	—	—	—	—	—
B1	40 mm steel	1	367.1	0.38	966.05	44.8	42.5	0.12	0.12	8.20	8.54	7.82	8.16
8	40 mm steel	1.5	—	—	—	—	—	—	—	—	—	—	—
9	40 mm steel	1	—	—	—	—	—	—	—	—	—	—	—
B2	35 mm ply	1.5	118.6	2.9	40.9	56.9	49.6	0.48	0.42	9.66	9.91	6.76	7.01
11	35 mm ply	2	117.6	2.7	43.55	60.8	55.2	0.52	0.47	10.72	10.58	8.02	7.88
B3	35 mm ply	2	—	—	—	—	—	—	—	—	—	—	—
13	35 mm ply	2	124.5	2.18	57.11	57.4	58.8	0.46	0.47	10.92	10.89	8.74	8.71

the variation of the deflection measured at mid-span with the applied load. From the figure, it can be seen that the beam exhibited ductile behavior, with failure occurring after yielding of the longitudinal reinforcement bars at mid-span and the formation of extensive flexural cracking outside the mid-span region; loss of load-carrying capacity eventually occurred after longitudinal splitting followed by crushing of concrete within the mid-span region of the compressive zone. The exhibited mode of failure and the experimentally established load-carrying capacity are in line with predictions obtained from EC2 (2004).

## 4 | SPECIMEN BEHAVIOR UNDER DROP-WEIGHT LOADING

During drop-weight testing, attention is focused on establishing the variation of the behavioral characteristics of the specimens throughout the loading process. Depending on the type of pad used in the impact region, the impact tests carried out have been categorized as high and medium (moderate) intensity impact tests.

### 4.1 | Impact force and support reactions

The curves presented in Figure 6 show the variation of the impact and support reactions during the first 40 ms (0.04 s) of each impact (drop-weight) test, starting just before the moment of contact between the impactor and the specimen and finishing when the values of the impact and support reactions become a small fraction of their peak values. It should be noted that, due to instrumentation failure, the figure does not include data from tests 6, 8, 9, and 10 (see Table 1). However, information for these tests has been obtained from the high speed camera and discussed later.

From Figure 6, it can be seen that the impact force increases rapidly (immediately after the drop-mass comes into contact with the specimen) to a maximum value and then rapidly reduces. It is interesting to note that the variation of the impact force with time is characterized by multiple peaks which are likely to be associated with secondary impacts and reflect the effect of cracking of concrete in the impacted region (scrubbing). The curves describing the time history of the support reactions reveal that the latter start increasing with a delay when compared to the contact forces measured in the impacted region. This delay reflects the time required by the stress waves, generated during impact, to reach the supports. It is also interesting to note that the curves describing the time history of the support reactions are also

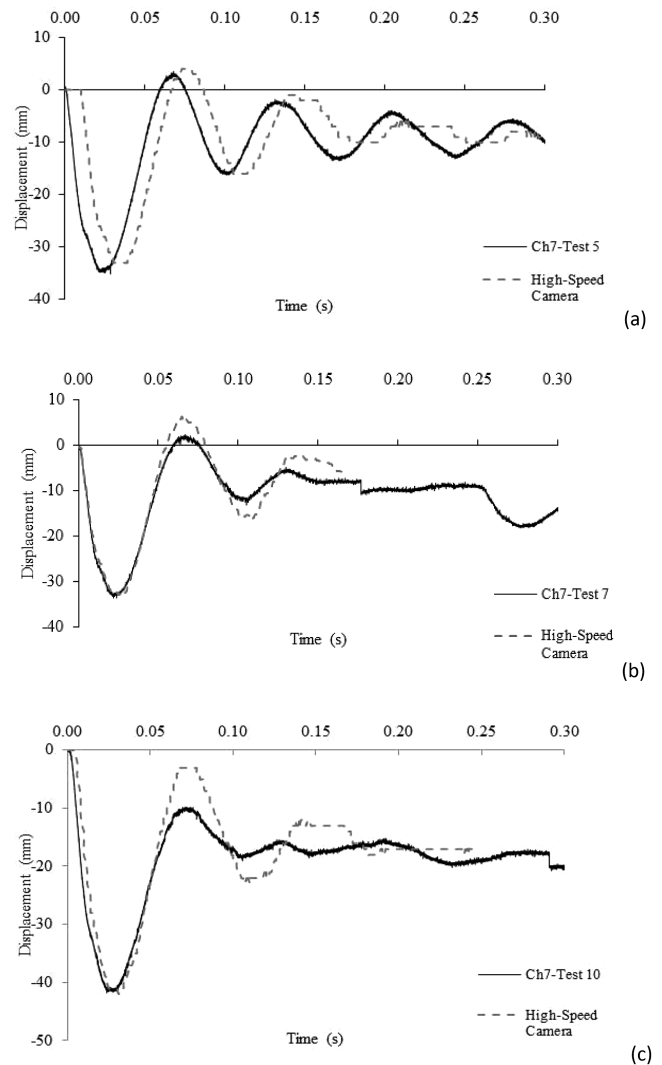


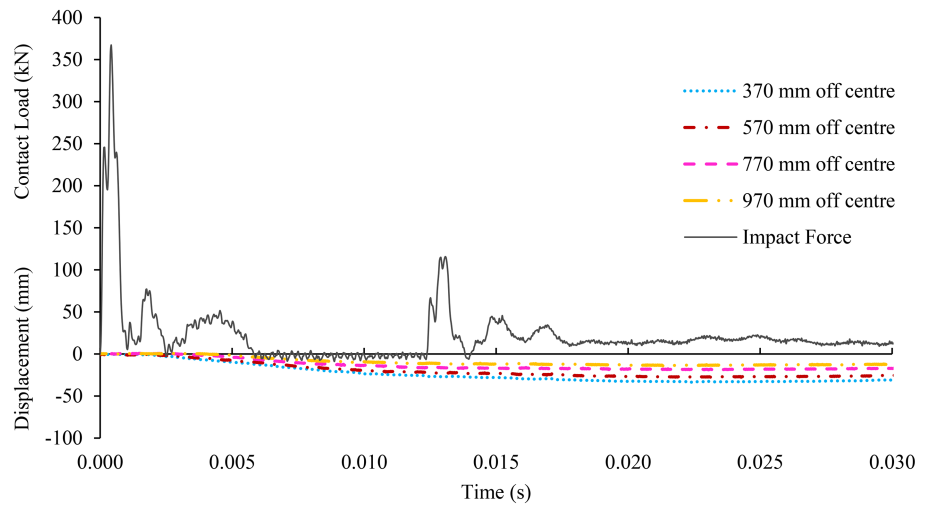
**FIGURE 7** Correlation between the displacement time histories obtained during droppedweight testing from the LVDT (CH-7) and the analysis photographic evidence obtained from the HS camera for (a) test 5, (b) test 7 and (c) test 10

characterized by multiple peaks due to the secondary impacts referred to earlier and the oscillation exhibited by the specimen.

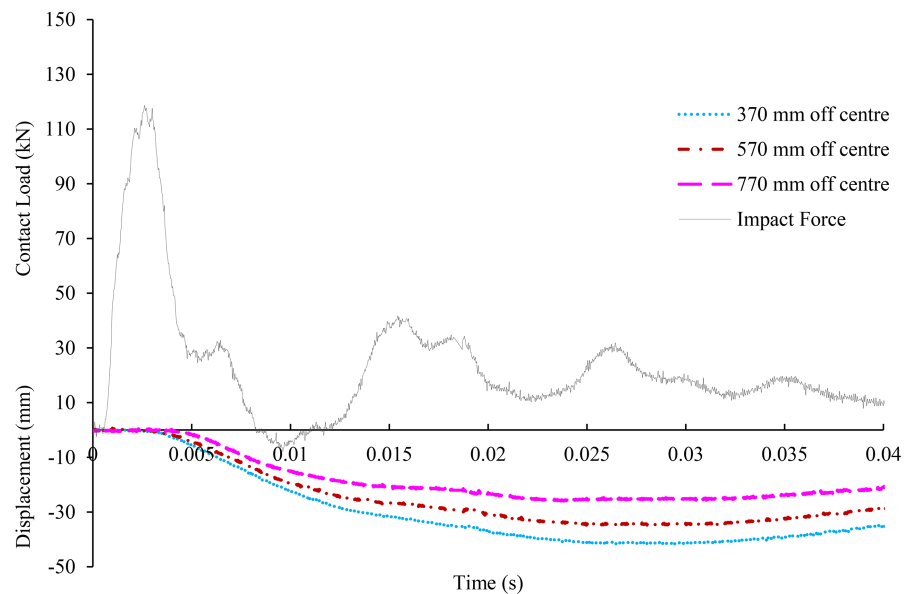
On the basis of the information presented in Figure 6, a number of key parameters are identified. These include the peak values (intensities) of the impact force ( $maxP_d$ ) and support reactions ( $maxR_d$ ) measured during testing and the corresponding time  $t_p$  and  $t_R$ , respectively, at which these values are attained, the average loading rate  $\dot{P} = maxP_d/t_p$  and the time interval (delay)  $\Delta t_{P-R} = t_R - t_p$  between  $maxP_d$  and  $maxR_d$ . The values of the above parameters are provided in Table 3. It is noted that in some cases data is missing due to instrumentation failure when conducting the impact tests (e.g., tests 6 and 8).

From Table 3, it can be seen that the 40 mm steel pads placed between the steel drop mass and specimens

**FIGURE 8** Impact force and displacement time histories obtained from (a) high (test 7) and (b) medium (test 10) intensity drop weight testing



(a) Test 7



(b) Test 10

A3 and B1 (high-intensity impact) resulted in values of  $maxP_d$  and loading rate  $\dot{P}$  significantly larger than their counterparts resulting from the tests on specimens A2, B2, and B3 for which the plywood pads used resulted in softer impact (moderate-intensity impact). The test data obtained from the high-intensity impact tests (steel pads) reveals a considerable difference between the values  $maxP_d$  and  $maxR_d$  (i.e., the sum of the values at the two supports) which is reflected in the small values ( $0.15 + 0.14 = 0.29$  and  $0.12 + 0.12 = 0.24$ ) of the ratio  $maxR_d/maxP_d$  in Table 3. Such small values of this ratio are considered to indicate that a large portion of the impact energy is consumed into causing the cracking suffered by the specimens. On the other hand, for the case of the moderate-intensity impact test (plywood pads), the deviation of the values of  $maxP_d$  from those of  $maxR_d$  is small (in Table 3,  $maxR_d/maxP_d$  ranges between 0.65 for test

3 to 0.99 for test 10) and this is considered to indicate that the transfer of the load from the impacted region to the supports is accomplished without significant loss of energy in the form of cracking. It would appear from the above, therefore, that such difference in the behavior resulting from high-intensity and moderate-intensity impact tests reflects the level of damage suffered by the specimens in the form of cracking.

It is also worth noting that the time interval  $\Delta t_{P-R} = t_R - t_P$  between the time at which  $maxP_d$  and  $maxR_d$  are attained increases as the intensity of the impact force and the level of damage suffered by the specimens increases. This becomes apparent by comparing the values of  $\Delta t_{P-R}$  for specimens A2 and B2 which, as Table 1 indicates, were tested more than once. From the table, it can be seen that specimen A2 was tested three times, with the applied load being dropped from

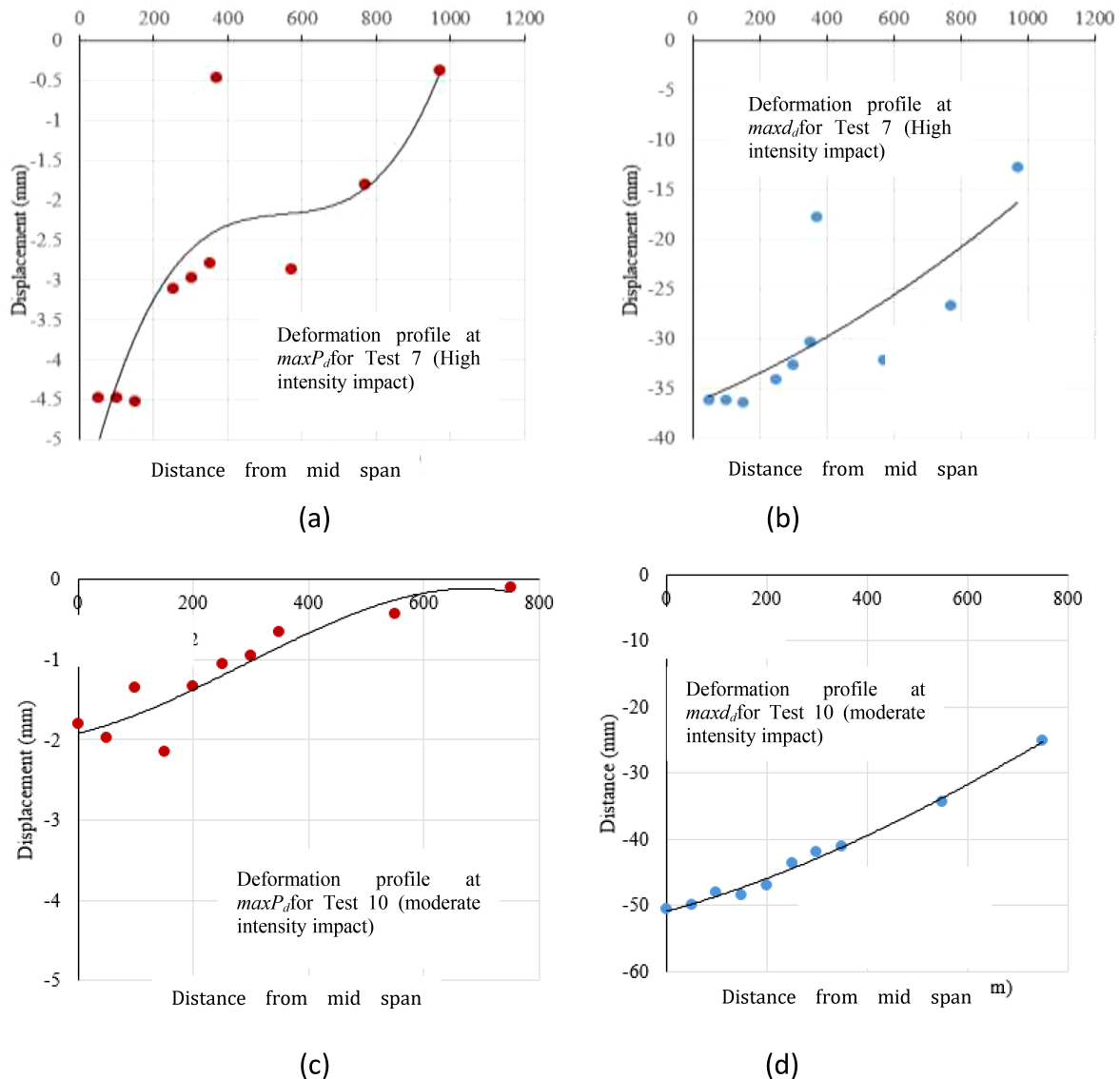


**FIGURE 9** Deformation profile of the RC beam specimen established through the combined use of a HS camera and LVDTs when (a, c)  $maxP_d$  and (b, d)  $maxd_d$  are attained for the case of high (tests 7) and moderate (test 10) intensity impact

heights 0.5, 1 and again 1 m, whereas beam B2 was tested twice, with the applied load being dropped from heights of 1.5 and 2 m. As a result, the damage suffered by the specimens increases with the number of tests carried out and this is reflected in the increase of  $\Delta t_{P-R}$  indicated in Table 3 when comparing the values obtained from the consecutive tests 2, 3 and 4 for specimen A2 and tests 10 and 11 for specimen B2.

## 4.2 | Displacement data and deformation profiles

Figure 7 shows that the displacement time histories measured at a distance of 370 mm from the specimen mid span through the use of LVDTs correlate very closely

with their counterparts established through the use of the high speed video camera. From the figure, it can be seen that, after the initial contact between impactor and specimen, the deflection of the specimens increases to a maximum value and, following a number of fluctuations for a short period, obtains its residual value, the latter essentially being dependent on the level of damage suffered by the specimens. Moreover, by comparing the peak values of load and deflection shown in Figures 6 and 7, respectively, it is interesting to note that the deflection reaches its maximum value well after the peak impact load is attained.

Figure 8 shows the time-histories of (a) the displacements measured by the LVDTs along the span of beams 7 and 10, and (b) the corresponding contact force. From the figure, it can be seen that, when the maximum

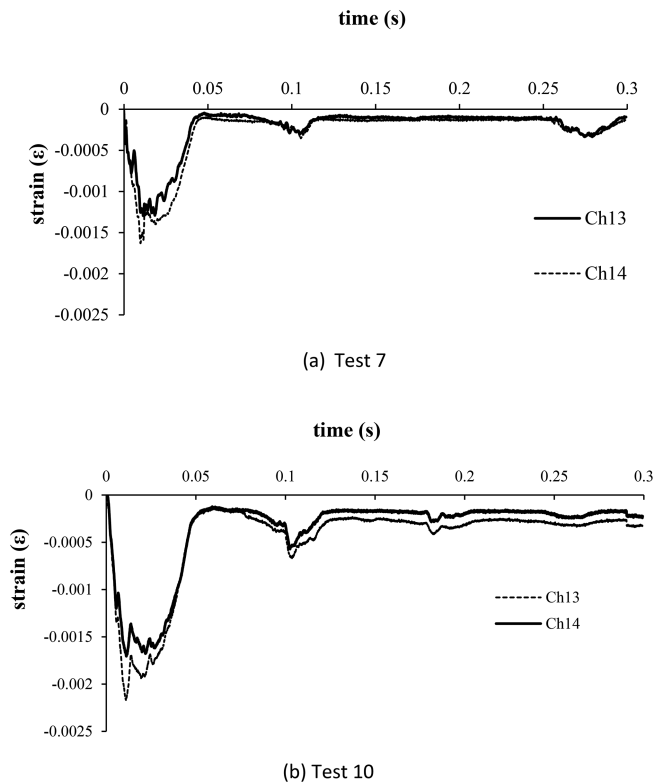


**FIGURE 10** Variation of strain measurements obtained from the strain gauges for the case of (a) high (tests 7) and (b) medium (test 10) intensity impact

impact load ( $maxP_d$ ) is attained, the deflections of the RC beam, even at mid-span, are a small fraction of the maximum displacement measured during testing. This indicates that during the initial stages of the loading process (prior to  $maxP_d$  being attained) the specimens exhibit localized response with the impact load essentially being resisted by a small portion of the beam's mid-span impacted region. Finally, it is noted that the residual values of the impact force (see Figure 8) are approximately equal to the weight of the drop-hammer (124 kgr) used to conduct the drop test.

An indication of the localized response may also be obtained from the deformation profiles (presented in Figure 9) of the portion of the beam between mid-span and the right-hand-side support for the cases of high- and medium-intensity impact (tests 7 and 10, respectively). From the figure, it can be seen that, unlike the smooth variation of the deflection along the beam span exhibited by the deformation profiles established directly from the LVDT readings, the deformation profiles established by calculation through the use of the digitized video recordings exhibit some discrepancies, inherent in the method of calculation, without, however, causing any significant deviation from the trends of behavior established from the LVDT readings. On

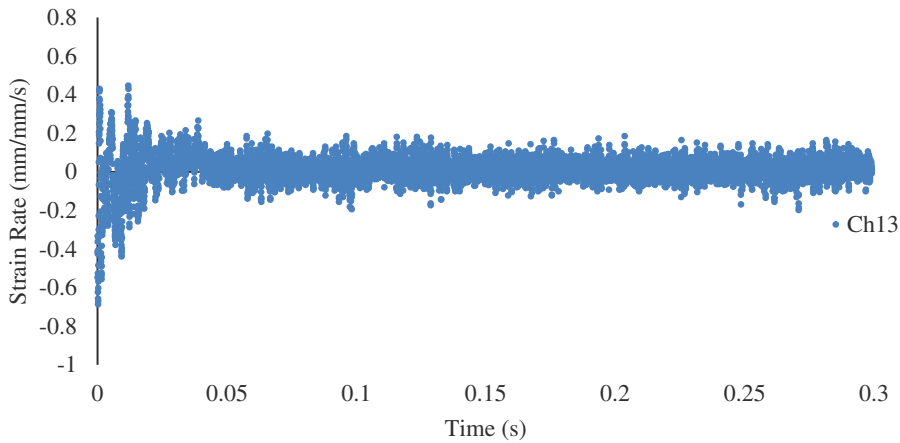
the basis of these deformation profiles it can be seen, yet again, that during the initial stages of the loading process (approximately up to the time at which  $maxP_d$  is attained) the RC beams exhibit “localized” response, in that only the portion of the span of the specimen close to the impacted region essentially reacts to the imposed load. However, when the maximum value of deflection at mid-span is attained (well after  $maxP_d$  is reached) the full length of the specimens deforms exhibiting “global” response. It is interesting to note that for the case of Test 7, which is characterized by higher values of loading rate and intensity, the “localized” response is more pronounced as the values of deflection associated with  $maxP_d$  are considerably higher than those established in the case of Test 10 (the latter test being characterized by lower levels of intensities and rates of loading).

### 4.3 | Strains and strain rates

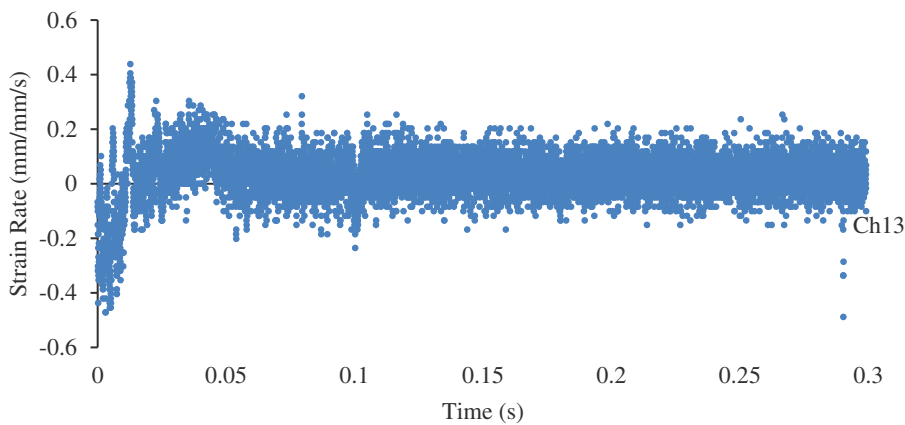
The variation of the strain ( $\epsilon$ ) values measured on, or close to, the top face of the beam at a distance of 260 mm from mid-span and the corresponding calculated values of the strain rates ( $\dot{\epsilon}$ ) are presented in Figures 10 and 11, respectively, for the cases of high- and medium-intensity impact (tests 7 and 10). From Figure 10, it can be seen that the peak values of strain are attained a few msec after the impactor comes into contact with the specimen, approximately at the same time at which the impact load attains its peak value ( $maxP_d$ ) (see Figure 6) and not when the maximum deflection ( $maxd_d$ ) is reached (well after  $maxP_d$  is attained). This essentially suggests the development of higher internal actions during the initial stages of the loading process when a localized response is exhibited. As regards the strain rate values shown in Figure 11, these appear to be small, not exceeding  $0.6 \text{ s}^{-1}$ .

An estimate of the longitudinal strains along the height of the beams in the mid-span region was made by analyzing the photographic data obtained from the high-speed camera. This was achieved by calculating the change in distance between successive grid points (shown in Figure 12) on the side face of each specimen tested. It should be noted that the photographic method employed cannot be used to measure the values of strain between points G and H (shown in Figure 12 to be located close to the top face of the specimen) as the relevant movement of these points is small. The time history of the calculated strains for the cases of high- and medium intensity impact (tests 7 and 10, respectively) are presented in Figure 13. From the figure, it can be seen that positive values of strain (indicating tension) develop nearly



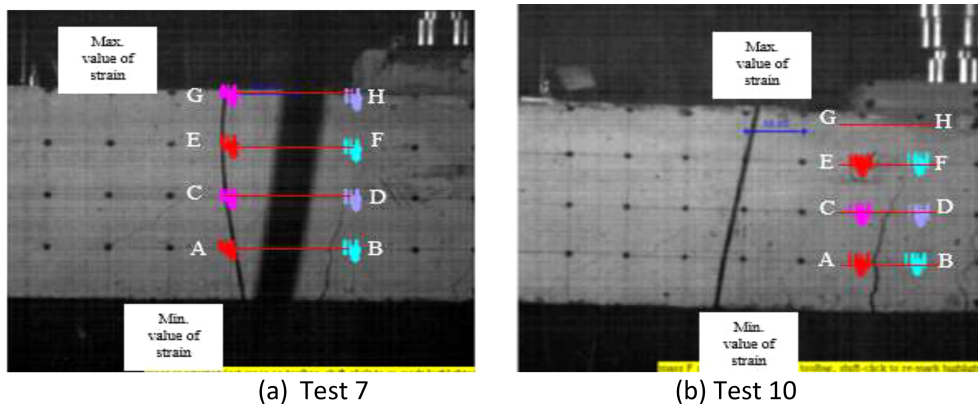


(a) Test 7



(b) Test 10

FIGURE 11 Variation of strain-rates obtained from the strain gauges for the case of (a) high (tests 7) and (b) medium (test 10) intensity impact



(a) Test 7

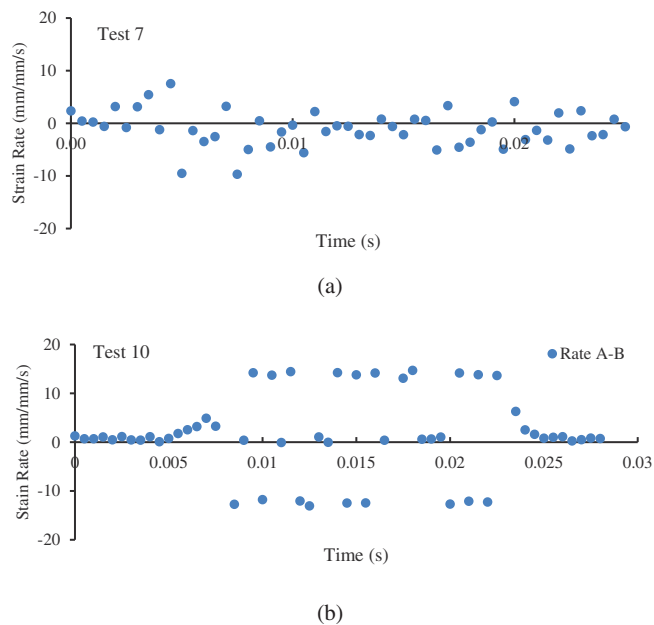
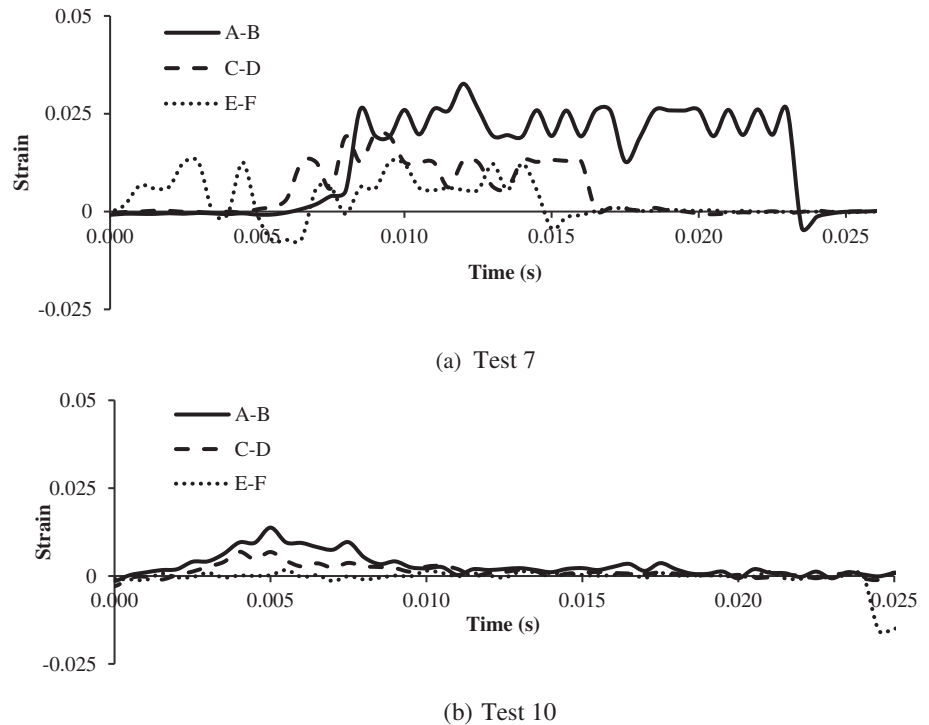
(b) Test 10

FIGURE 12 Selected points along the specimen height close to the impacted (mid-span) region

throughout the specimen height, whereas negative values of strain (indicating compression) are only measured close to the top face of the specimen (see Figure 10) even during the initial stages of the loading process. This shows that cracking develops and propagates deep into the compressive zone even before the impact load attains its peak value.

Figure 14 provides an estimate of the variation of the values of the strain-rate exhibited along the height of the specimen close to the mid-span region throughout the loading process. The calculation of these values was based on the values of strain shown in Figure 13. Figure 14 shows that the maximum values of the strain rate close to bottom surfaces of the beam is  $10 \text{ s}^{-1}$ , for test

**FIGURE 13** Curves describing the time histories of strain along the height of the specimen close to the impacted mid-span region between the points shown in Figure 12 for: (a) test 7 and (b) test 10



**FIGURE 14** Variation with time of the strain -rate exhibited between points a and B at the bottom face of the beam mid -span (see Figure 12) for (a) test 7 and (b) test 10

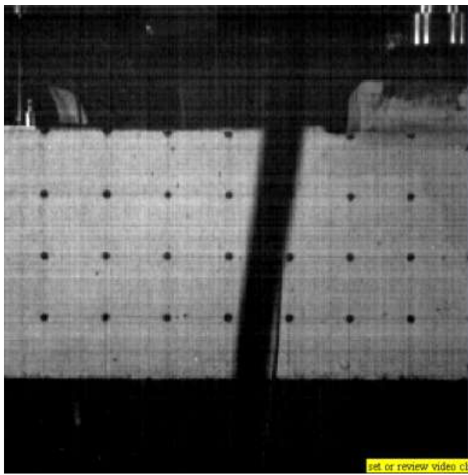
7, and  $15 \text{ s}^{-1}$  in the case of test 10. Nevertheless, it is important to point out that the higher tensile values of strain rate which developed during testing are mainly associated with flexural cracking in the mid-span region that penetrated deep into the compressive zone during the initial stages of the loading process (i.e., before  $\max P_d$  is attained). As a result, it could be suggested that high

values of strain-rate in the region of the specimen in tension are likely to reflect the rate at which the cracks widen rather than the actual deformation of concrete.

#### 4.4 | Cracking process and mode of failure

Photographs obtained from the high-speed camera at different stages of the loading process for high- and moderate-intensity impact (tests 7 and 10) are presented in Figures 15 and 16, respectively. It is noted that the high-speed camera focused on the left-hand-side portion of the specimens, between the mid-span region and the left support. The photographs presented in Figure 15 show that cracking occurred immediately after the impactor came into contact with the top surface of the RC beam at mid span. From these photographs, it appears that inclined cracks form and quickly extend towards the upper face of the specimen very early in the loading process, prior to the contact (impact) force attaining its peak value ( $\max P_d$ ).

From Figure 8 describing the variation with time of (a) the contact force and (b) the deflection established by the LVDT measurements taken along the span of the beam, it is clear that when the maximum impact load ( $\max P_d$ ) is attained, the deflection exhibited by the RC beam is a small fraction of the maximum deflection measured during testing. The fact that cracking is exhibited early in the loading process, prior to  $\max P_d$  being



(a) (immediately before contact)

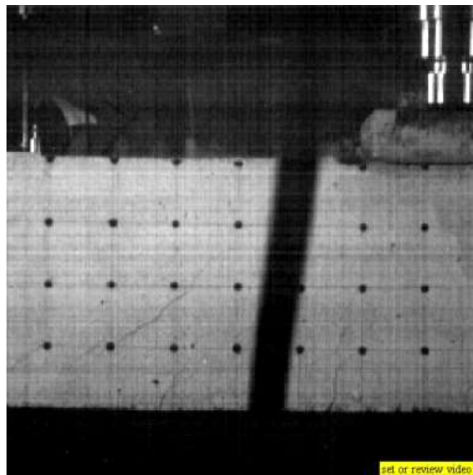
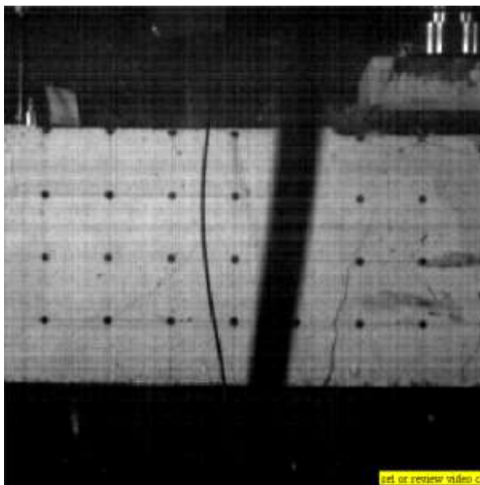
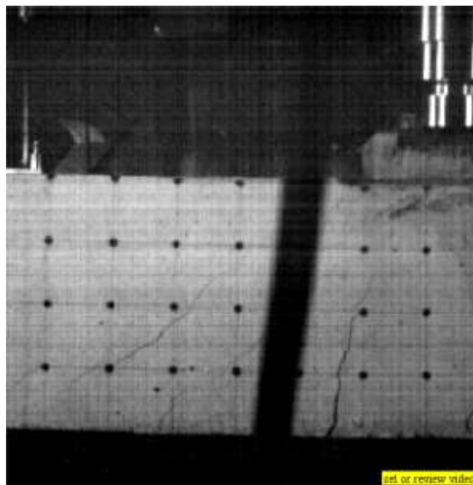
(b)  $t_p = 0.38$  msec (at  $maxP_d$ )(c)  $t = 1$  msec (uplift of the impactor)(d)  $t_{d,max} = 22$  msec (at maximum mid-span deflection)

FIGURE 15 Cracking process of RC beam under high-intensity impact (tests 7)

achieved, confirms (once again) that the specimen exhibits localized response with only a small portion of the beam span, in the mid-span region, reacting to the imposed load.

Under static loading, all specimens considered in this study are expected to exhibit the ductile behavior experimentally established for beam specimen A1 (see Figure 5). Under impact loading, however, the cracking is more localized, primarily occurring around the mid-span impacted region often resulting in brittle, and sometimes explosive, type of failure. Furthermore, another set of cracks initiates at the upper face of the beams, at a certain distance from the mid-span, and extends vertically towards the specimens' bottom face (see Figures 17 and 18). These crack patterns are in line with the results of previous experimental work<sup>1,3-6,8,9</sup> and numerical work,<sup>15,18</sup> which essentially define the portion of the RC beam (effective length,  $L_{eff}$ ) primarily reacting to the imposed impact load.<sup>15,18,21</sup>

After the maximum impact force ( $maxP_d$ ) is attained (0.38 and 4.05 ms after contact of the drop mass and the specimen as indicated in Figures 15 and 16 for tests 7 and 10, respectively), the cracks that developed up to this stage continue to widen and further extend into the compressive zone as the deflection of the RC beam increases due to inertia. In some cases cracking results in extensive disintegration of concrete and this often causes the beam to rely on post-failure mechanisms for the transfer of the applied load to the supports, particularly when conducting consecutive drop-weight tests on the RC beam specimens. This can be seen by reference to Figures 17 and 18 which show the crack pattern of specimens B2 and B3 at the end of two successive drop tests. It becomes clear from these crack patterns, which, in Figures 17a and 18a, are characterized by deep flexural cracking combined with horizontal splitting in the mid span impacted region, that both specimens attained their flexural

**FIGURE 16** Cracking process of RC beam under moderate -intensity impact (test 10)

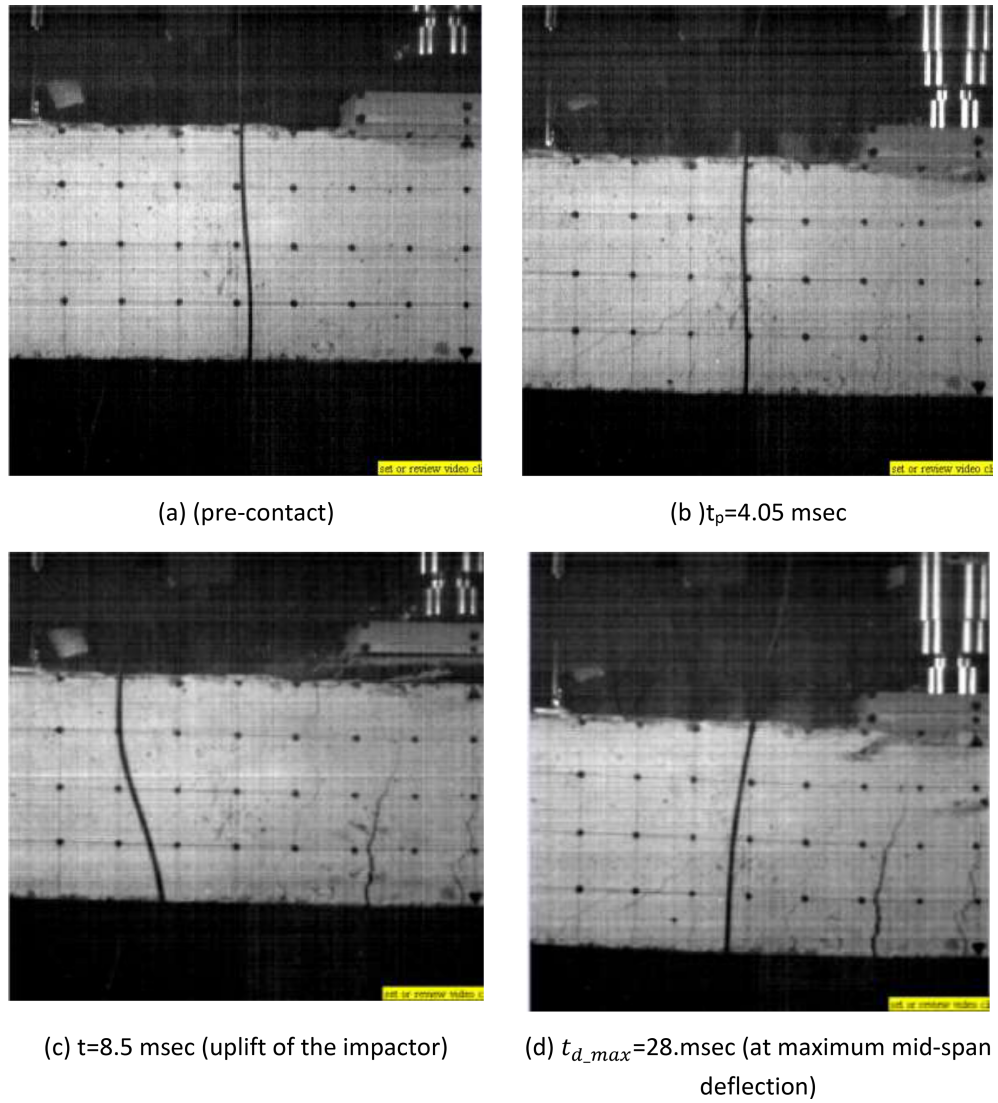
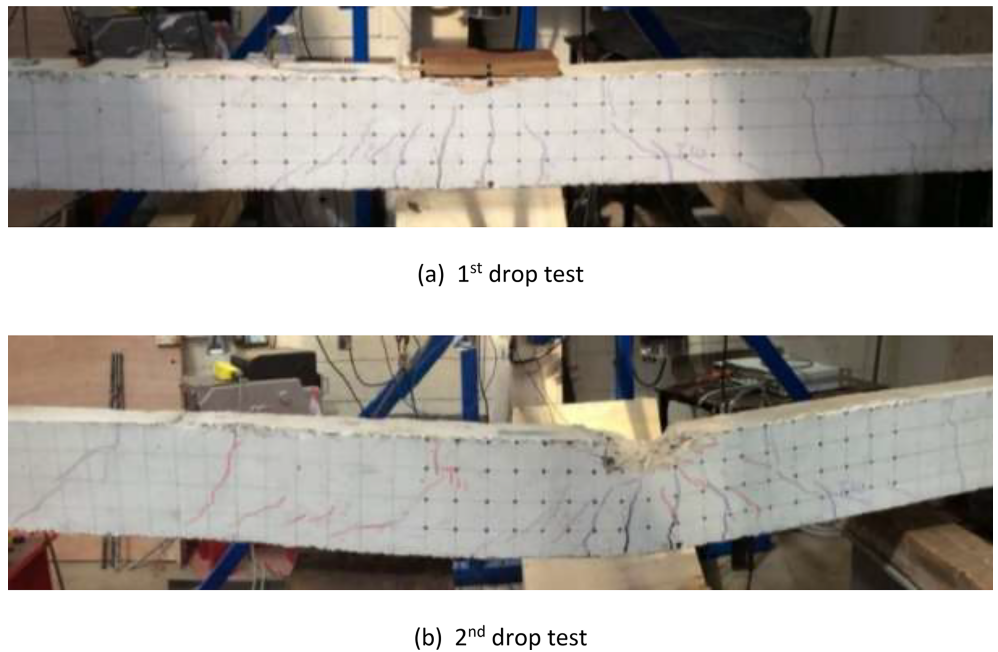


**FIGURE 17** Crack pattern of specimen B2 at the end of (a) the first (test 10, see Table 3) and (b) the second (test 11, see Table 3) drop test





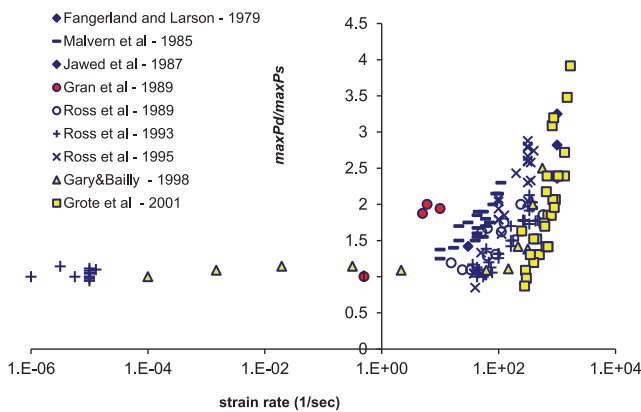


(a) 1<sup>st</sup> drop test

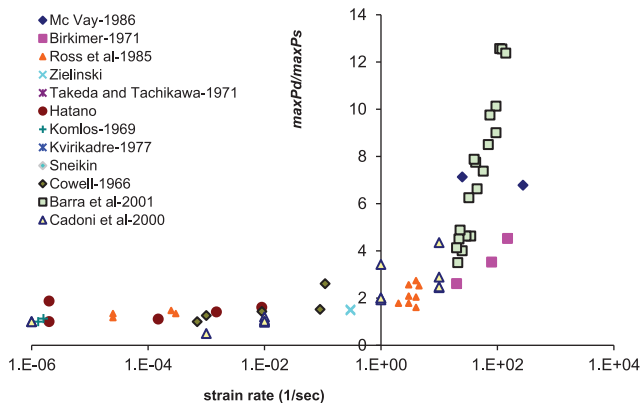


(b) 2<sup>nd</sup> drop test

FIGURE 18 Crack pattern of specimen B3 at the end of (a) the first (test 12, see Table 3) and (b) the second (test 13, see Table 3) drop test



(a)



(b)

FIGURE 19 Experimental data obtained from experiments conducted on plain concrete specimens subjected to high rates of uniaxial (a) compression and (b) tension loading

capacity during the first drop test. Therefore, the specimens' load-carrying capacity should be considered thereafter lost for any practical purpose, since load transfer by beam action is not any more possible. As a result, although for both specimens the value of  $maxP_d$  measured during the second drop test was similar to that measured during the first, the data obtained should not be considered as meaningful for practical structural applications. The same reasoning appears realistic to apply for data obtained for a single drop test after the time at which the specimen crack pattern indicates that flexural capacity has been attained.

## 5 | DISCUSSION-DESIGN IMPLICATIONS

The data presented in Figure 19 has been extracted from Cotsovos and Pavlović.<sup>26-28</sup> They have been obtained from tests carried out on concrete prisms under uniaxial compression and tension, respectively, through the use of the Split Hopkinson Pressure Bar (SHPB) apparatus and describe the variation of the strength of concrete specimens with the rate of loading. From the figures, it can be seen that an increase in specimen strength is exhibited once certain thresholds of strain rate are surpassed. These are approximately 100 and  $10\text{ s}^{-1}$  for uniaxial compression and tension, respectively. In the case of compression, comparing these thresholds with the values of strain rate characterising RC behavior under drop-weight loading (presented in Figure 14) shows that, the latter values are significantly smaller and, thus, strain-rate effects are not likely to result in an increase of compressive concrete strength that could, in turn, affect beam structural behavior. Furthermore, when



considering tension, high values of strain rate are measured after the development of cracking on the beams and therefore describe the rate at which the widths of the cracks increase rather the rate of concrete material deformation. Such observations are in conflict with current design practice, as reflected in codes of practice predominantly concerned with the design of military structures (e.g., TM5-855-1<sup>23</sup>), which attribute the increase of load-carrying capacity of RC structures under impact loading to the strain-rate sensitivity of the materials used.

An alternative explanation for the effect of the rate of loading on load-carrying capacity has been provided in Cotsovos et al.<sup>15</sup> and Cotsovos<sup>21</sup> and this is consistent with the experimental information presented herein. As discussed in Section 4.2 by reference to Figure 8, the impact force attains its peak value soon after contact of the drop-weight with the beam. Once this load value is attained, the deformation profiles of the beams presented in Figure 10 show that deflection reduces rapidly with the distance from the impacted mid span and becomes practically zero well before the supports. Moreover, as indicated in Figure 18, the location at which the deflection diminishes to zero is marked by the presence of a vertical crack which initiates at the top face of the beam and extends downwards. Therefore, it would appear from the above that resistance to the applied load is essentially provided by the portion of the beam extending, on either side of the mid-span, to the cross-section where vertical cracking initiates at the top face and extends downwards. This portion, which has been termed  $L_{eff}$  and proposed as the underlying cause of the increase of  $maxP_d$  with the rate of loading, has formed the basis of an alternative design method which is described in Cotsovos et al.<sup>15</sup> and Cotsovos.<sup>21</sup>

## 6 | CONCLUSIONS

From the work described above the following conclusions may be drawn:

It is confirmed that the rate of loading can lead to a significant increase of the load that can be sustained by RC beams when compared with their statically applied counterpart.

In contrast with the applied force which increases rapidly and attains its peak value immediately after the dropped mass comes into contact with the specimen, the support reactions start increasing with a delay reflecting the time required for the stress waves to reach the supports.

The intensity of impact depends on the pad placed between drop mass and specimen. A steel pad results in high-intensity impact, whereas a plywood pad results in moderate-intensity impact.

The sum of the maximum values of the support reactions is equal to a value of the order of 30% the peak value of the impact load for the case of high-intensity impact, whereas, for moderate-intensity impact, it varies between 35% and nearly 100%. Such difference in behavior is considered to reflect the energy consumed to cause the damage suffered by the specimens in the form of cracking.

Both the conventional instrumentation (LVDTs) and the high-speed video camera produced similar displacement time histories. It was found that deflection at mid span attains its peak value significantly later than the peak value of the applied (impact) load; when the impact load attains its peak value, the deflection is only a small fraction of its peak value.

From the deformation profile of the specimens up to the time the impact load attains its peak value, it appears that only the portion of the beam in the mid-span impacted region responds to the impact load. However, this “localized response” becomes “global” as the full length of the specimen deforms with the mid-span deflection attaining its peak value well after the peak value of the impact load is reached.

The strain rates measured at the mid-span region of the beam are significantly smaller than the threshold values which mark the start of a sharp increase in load-carrying capacity of prismatic specimens in compression or tension with strain rate. Assuming that that the increase of load-carrying capacity of the prismatic specimens indicates strain-rate sensitivity of concrete strength, the measured strain-rate values indicate that RC behavior is not affected by such a sensitivity.

The test data obtained from impact tests on RC beams after the time at which the experimentally established crack pattern indicates that flexural capacity is attained should not be considered useful for practical structural applications.

## DATA AVAILABILITY STATEMENT

All data referred to in this publication are available upon request from the corresponding author.

## ORCID

Demitrios M. Cotsovos  <https://orcid.org/0000-0002-7258-5031>

## REFERENCES

1. Hughes G and Spiers DM. An investigation on the beam impact problem. Technical Report 546. London: Cement and Concrete Association; 1982. p. 117.
2. Kulkarni SM, Shah SP. Response of reinforced concrete beams at high strain rates. ACI Struct J. 1998;95(6):705–15.
3. Miyamoto A, King M, Fujii M. Non-linear dynamic analysis and design concepts for RC beams under impulsive loads. Bull N Zeal Natl Soc Earthquake Eng. 1989;22(2):98–111.

4. Kishi N, Mikami H, Matsuoka KG, Ando T. Impact behaviour of shear-failure-type RC beams without shear rebar. *Int J Impact Eng.* 2002;27(9):955–68.
5. Kishi N, Mikami H, Ando T. An applicability of the FE impact analysis on shear-failure-type RC beams with shear rebars. *Proceedings of the 4th Asia-Pacific Conference on Shock and Impact Loads on Structures.* Singapore; CI-Premier; 2001. p. 309–15.
6. May IM, Chen Y, Owen DRJ, Feng YT, Thiele PJ. Reinforced concrete beams under drop-weight impact loads. *Comput Concr.* 2006;3(2–3):79–90.
7. Fujikake K, Li B, Soeun S. Impact response of reinforced concrete beam and its analytical evaluation. *ASCE J Struct Eng.* 2009;135(8):938–50.
8. Saatci S, Vecchio FJ. Effects of shear mechanisms on impact behaviour of reinforced concrete beams. *ACI Struct J.* 2009a;106(1):78.
9. Saatci S, Vecchio FJ. Nonlinear finite element modeling of reinforced concrete structures under impact loads. *ACI Struct J.* 2009b;106(5):717.
10. Abbas AA, Pullen AD, Cotsovos DM. Structural response of RC wide beams under low-rate and impact loading. *Magazine of Concrete Research.* 2010;62(10):723–740. <http://doi.org/10.1680/macr.2010.62.10.723>.
11. Adhikary SD, Li B, Fujikake K. State-of-the-art review on low-velocity impact response of reinforced concrete beams. *Magaz Concr Res.* 2015;68(14):701–23.
12. Anil O, Durucan C, Erdem RT, Yorgancilar MA. Experimental and numerical investigation of reinforced concrete beams with variable material properties under impact loading. *Construct Build Mater.* 2016;125:94–104.
13. Thabet A, Haldane D. Three-dimensional simulation of nonlinear response of reinforced concrete members subjected to impact loading. *ACI Struct J.* 2000;97(5):689–702.
14. Abbas H, Gupta NK, Alam M. Nonlinear response of concrete beams and plates under impact loading. *Int J Impact Eng.* 2004;30(8):1039–53.
15. Cotsovos DM, Stathopoulos ND, Zeris CA. Behaviour of RC beams subjected to high rates of concentrated loading. *ASCE J Struct Eng.* 2008;134(12):1839–51.
16. Kishi N, Khasraghy SG, Kon-No H. Numerical simulation of reinforced concrete beams under consecutive impact loading. *ACI Struct. J.* 2011;108(4):444.
17. Adhikary SD, Li B, Fujikake K. Dynamic behaviour of reinforced concrete beams under varying rates of concentrated loading. *Int J Impact Eng.* 2012;47:24–38.
18. Cotsovos DM, Pavlović MN. Modelling of RC beams under impact loading. *ICE Proc Struct Build.* 2012;165(2):77–94.
19. Pham TM, Hao H. Prediction of the impact force on reinforced concrete beams from a drop weight. *Adv Struct Eng.* 2017;9(11):1–14.
20. Guo J-L, Cai J, Zuo Z-L. Simplified dynamic analysis of reinforced-concrete beams under impact actions. *Proc Inst Civil Eng Struct Build.* 2017;170(3):211–24.
21. Cotsovos DM. A simplified approach for assessing the load-carrying capacity of reinforced concrete beams under concentrated load applied at high rates. *Int J Impact Eng.* 2010;37:907–17.
22. Kotsovos MD. *Compressive force-path method unified ultimate limit-state design of concrete structures.* 1st, Switzerland: Springer International Publishing; 2014.
23. TM5-855-1, 1998. “Design and analysis of hardened structures to conventional weapons effects.” The Departments of Army, Air Force and Navy and the Defence Special Weapons Agency, New York.
24. EN 1992-1-1. *Eurocode 2: Design of concrete structures. Part 1-1: General rules and rules for buildings.* Brussels: CEN; 2005.
25. Tracker 4.87. (2014). Brown.D.
26. Cotsovos DM, Pavlović MN. Numerical investigation of concrete subjected to compressive impact loading. Part 1: a fundamental explanation for the apparent strength gain at high loading rates. *Comput Struct.* 2008a;86(1):145–63.
27. Cotsovos DM, Pavlović MN. Numerical investigation of concrete subjected to compressive impact loading. Part 2: parametric investigation of factors affecting behaviour at high loading rates. *Comput Struct.* 2008b;86(1):164–80.
28. Cotsovos DM, Pavlović MN. Numerical investigation of concrete subjected to high rates of uniaxial tensile loading. *Int J Impact Eng.* 2008c;35(5):319–35.

## AUTHOR BIOGRAPHIES



Noosha Madjlessi  
BEng, MSc, PhD  
Institute of Infrastructure and Environment  
Heriot-Watt University  
Edinburgh EH14 4AS, UK



Demitrios M. Cotsovos  
Dipl Ing, MSc, DIC, PhD, CEng  
Associate Professor  
Institute of Infrastructure and Environment  
Heriot-Watt University  
Edinburgh EH14 4AS, UK

[d.cotsovos@hw.ac.uk](mailto:d.cotsovos@hw.ac.uk)



Mojtaba Moatamedi  
BEng, MSc, MBA, LL.M., PhD,  
MASME, FRAeS, FNuCI  
Professor  
Faculty of Technology, Art and Design  
Oslo Metropolitan University

Oslo, Norway

**How to cite this article:** Madjlessi N, Cotsovos DM, Moatamedi M. Drop-weight testing of slender reinforced concrete beams. *Structural Concrete.* 2021;22:2070–2088. <https://doi.org/10.1002/suco.202000395>